We are IntechOpen, the world's leading publisher of Open Access books Built by scientists, for scientists

6,900
Open access books available

185,000
International authors and editors

200M
Downloads

154
Countries delivered to

Our authors are among the

TOP 1%
most cited scientists

12.2%
Contributors from top 500 universities

CLARIVATE ANALYTICS
BOOK
CITATION
INDEX
INDEXED

WEB OF SCIENCE™

Selection of our books indexed in the Book Citation Index
in Web of Science™ Core Collection (BKCI)

Interested in publishing with us?
Contact book.department@intechopen.com

Numbers displayed above are based on latest data collected.
For more information visit www.intechopen.com

Quantum Physical Interpretation of Thermoelectric Properties of Ruthenate Pyrochlores

Sepideh Akhbarifar

Abstract

Lead- and lead-yttrium ruthenate pyrochlores were synthesized and investigated for Seebeck coefficients, electrical- and thermal conductivity. Compounds $A_2B_2O_{6.5+z}$ with $0 \leq z < 0.5$ were defect pyrochlores and p-type conductors. The thermoelectric data were analyzed using quantum physical models to identify scattering mechanisms underlying electrical (σ) and thermal conductivity (κ) and to understand the temperature dependence of the Seebeck effect (S). In the metal-like lead ruthenates with different Pb:Ru ratios, $\sigma\,(T)$ and the electronic thermal conductivity $\kappa_e\,(T)$ were governed by 'electron impurity scattering', the lattice thermal conductivity $\kappa_L\,(T)$ by the 3-phonon resistive process (Umklapp scattering). In the lead-yttrium ruthenate solid solutions ($Pb_{(2-x)}Y_xRu_2O_{(6.5\pm z)}$), a metal–insulator transition occurred at 0.2 moles of yttrium. On the metallic side (<0.2 moles Y) 'electron impurity scattering' prevailed. On the semiconductor/insulator side between x = 0.2 and x = 1.0 several mechanisms were equally likely. At x > 1.5 the Mott Variable Range Hopping mechanism was active. $S\,(T)$ was discussed for Pb-Y-Ru pyrochlores in terms of the effect of minority carrier excitation at lower- and a broadening of the Fermi distribution at higher temperatures. The figures of merit of all of these pyrochlores were still small ($\leq 7.3 \times 10^{-3}$).

Keywords: Ruthenate pyrochlores, thermoelectricity, scattering mechanisms, metal–insulator transition, glass-like thermal conductivities

1. Introduction

The discovery of high thermoelectric performance of Na_xCoO_4 [1] has triggered renewed interest in oxide thermoelectric materials, though the figure of merit (zT) of this and other oxides is still too small for widespread application.

Pyrochlore is an oxide mineral [$(Na,Ca)_2Nb_2O_6\,(OH,F)$] that forms brown to black, glassy octahedral crystals. In natural occurrences, the A and B atom sites can be occupied by many elements. Apart from naturally occurring compounds, over 500 compositions have been synthesized [2]. This wide-spread interest in pyrochlores is due to their large spectrum of properties, which include electronic, magnetic, electro-optic, piezoelectric, catalytic and more. The structure of pyrochlores is usually described by the topology and the geometric shape of coordination polyhedra. The structural formula is $^{VIII}A_2{}^{VI}B_2{}^{IV}X_6{}^{IV}Y$. The roman numerals show the coordination numbers. The crystal structure of pyrochlores is

face-centered cubic (fcc). The space group is *Fd3m*, the lattice parameter is a = 0.9-1.3 nm. There are 8 formula units in the unit cell. X is oxygen (O^{2-}) and Y can be oxygen, hydroxyl, fluoride (O^{2-}, OH^-, F^-). The unit cell contains larger A (r_A = 0.087 – 0.151 nm) and smaller B cations (r_B = 0.040 – 0.078 nm) [3] surrounded by oxygens; in minerals by some OH^- and/or F^-. The B atoms are accommodated in distorted, corner-sharing BO_6 octahedra. A network of BO_6 octahedra forms the backbone of the structure [4]. The larger A atoms are located inside of slightly distorted hexagonal rings formed by six BO_6 octahedra. The structure can be regarded as two interpenetrating networks of B_2O_6 and A_2O' units. The pyrochlore structure tolerates vacancies on the A and O' sites ('defect pyrochlores'), which can be represented by the general formula $A_{1-2}B_2X_6Y_{0-1}$. Work in this chapter deals with synthesizing lead ruthenate derivatives and lead-yttrium ruthenate solid solutions, measuring thermoelectric properties, and understanding the data based on the pyrochlore structure, A- and B-site occupancy, ligand and crystal fields as well as quantum-physical explanation of scattering mechanisms.

2. Electronic properties of ruthenate pyrochlores

Pyrochlores exhibit various electronic properties. Ruthenate pyrochlores with $4d$ transition elements on the B-site are of interest because their electronic properties can change when changing the A-site atom. The electrical conductivity is affected by the network of the corner-sharing RuO_6 octahedra, i.e., the B_2O_6 sublattice [4]. $Bi_2Ru_2O_7$ and $Pb_2Ru_2O_{6.5}$ show metal-like electrical conductivity to the lowest measured temperatures of a few degrees Kelvin [5, 6]. $Bi_2Pt_2O_7$ is an insulator [7]. $RE_2Ru_2O_7$ (rare earth RE = Pr to Lu), and $Y_2Ru_2O_7$ are Mott insulators with a spin-glass ground state [5, 8, 9]. Some pyrochlores show metal–insulator transitions (MIT), depending on temperature or pressure, for example $Hg_2Ru_2O_7$ and $Tl_2Ru_2O_7$ [10, 11]. $Tl_2Ru_2O_7$ shows a MIT at 120 K [9], likely due to the formation of a spin gap in the one dimensional Haldane chain [12]. Therefore, the electronic structure of a pyrochlore, especially near the Fermi level (E_F), must be affected by the element on the A-site via the A–O–Ru bond and the unoccupied O' sites. Defect pyrochlores are cationic conductors, i.e., they are solid electrolytes. Some of them with $4d$ or $5d$ atoms on the B-site have been used as oxygen electrodes, because of their ionic (O^{2-}) and electronic conductivity [4].

There are at least two factors that may contribute to the electronic properties of Ru(IV) pyrochlores: 1) The Ru–O–Ru bond angle, which affects the Ru^{4+} t_{2g} band width and varies with the size of the A-site cation [13]. 2) Hybridization of unoccupied states of A-site cations (e.g., Tl, Bi, and Pb) with the Ru $4d$ states via the oxygen framework [14]. Changes of the Ru–O–Ru bond angle depend also on the Ru–O bond length, which is affected by the size of A and the resulting changes in orbital overlap and bandwidth [13, 15]. Respective studies have shown that pyrochlores with metallic behavior have greater Ru–O–Ru bond angles than that of insulating ruthenate pyrochlores [16]. There seem to be only small structural changes in $A_2Ru_2O_7$ pyrochlores when comparing metallic and semiconducting members. Electrical transport properties may just be positioned near the edge of localized and itinerant electrons. This positioning at the edge of the metal–insulator divide may help finding promising thermoelectric materials. High Seebeck coefficients are on the insulator side and potentially acceptable electrical conductivity on the metallic side, providing a balance in properties [4, 5].

Lee et al. [13] computed the band width of Ru t_{2g} block bands for various pyrochlore ruthenates using the extended Hückel tight binding method and showed that metallic phases have a wider bandwidth than semiconducting phases. The

authors concluded that the metal-versus-insulator behavior of ruthenium pyrochlores can be explained in terms of the Mott-Hubbard mechanism of electron localization. Lee et al. [13] showed that there is a linear relationship between the ionic radius of the A cation and the Ru–O–Ru bond angle. I used the software *ATOMS V6.4.0* to calculate the Ru–O–Ru bond angle, which is 136.24°. The ionic radius for 8-coordinated Pb^{2+} is 0.129 nm. This is the highest bond angle and the largest ionic radius compared with the data shown in Figure 3a in [13]. The data confirm that Pb^{2+} follows as well the trendline established for cations on the A-site in ruthenate pyrochlores. Based on the high bond angle of 136.24°, $Pb_2Ru_2O_{6.5}$ can be expected to fall in the group of metallic ruthenate pyrochlore phases with a high Ru t_{2g} band width as shown by Lee et al. in Figure 3b in [13].

Lead ruthenate $Pb_2Ru_2O_{6.5}$ shows metal-like conductivity at room temperature. The ceramic has been used as catalyst for fuel cells, organic syntheses, and charge storage capacitors [4, 17]. As with all pyrochlores, the B atom, here Ru, is six-fold coordinated: each Ru atom is located at the center of a slightly distorted octahedron of equidistant oxygen atoms. Lead is VIII-coordinated with oxygen. $Pb_2Ru_2O_{6.5}$, or more precisely, $Pb_2Ru_2O_6O'_{0.5}$ forms an ordered defect-pyrochlore structure in which every other O′ site is empty [18]. The vacancies in the O′ sites are ordered. Following Hsu et al. [14] discussion, the metallic behavior of lead ruthenate is most likely due to the formation of an extended Pb 6p band overlapping with the Ru 4d band and is attributed to electron transport mainly within the octahedral network of BO_6 units, the backbone of the pyrochlore structure [4, 14, 19]. The fivefold Ru 4d levels are divided into an unoccupied e_g band ($\sim$ 2-5 eV above the Fermi energy E_F) and a partially occupied t_{2g} band ($\sim$ 1 eV below to 1 eV above E_F). The t_{2g} band is broad and mainly metallic due to covalent admixture with O 2p states. The Pb 6s state is too deep ($\sim$ 8.5-10 eV below E_F) to be mixed with the Ru 4d states (the Fermi levels are in the same partially filled Ru 4d band). However, the unoccupied Pb 6p bands (only 5-9 eV above E_F) are close enough to mix with the Ru 4d states.

3. Quantum physical background

Following semiconductor physics, transport theory of metals, and degenerate semiconductors (parabolic band, energy-independent scattering approximation [20]) the Seebeck coefficient S, the electrical resistivity ρ [21], and the total thermal conductivity κ can be expressed as

$$\sigma = \frac{1}{\rho} = \pm en\mu \tag{1}$$

$$S = \frac{8\pi^2 k_B^2}{3eh^2} m^* T \left(\frac{\pi}{3n}\right)^{2/3} \tag{2}$$

$$\kappa = \kappa_e + \kappa_L \tag{3}$$

where e is the charge of a carrier, n is the carrier concentration (1/m³), μ the carrier mobility (m²/V·s), and the plus or minus sign in Eq. (2) depends on the type of charge carrier, holes (+) or electrons ($-$); k_B is the Boltzmann constant, h is Planck's constant, T is the absolute temperature. The m^* in Eq. (2) refers to the effective mass of the charge carriers. Heavier carriers (higher m^*) will move more slowly. Hence, less mobility leads to lower electrical conductivity but a higher Seebeck coefficient (Eq. (2)). In other words, both, a smaller carrier concentration and a higher carrier's effective mass decrease electrical conductivity. The exact relationship between effective mass and carrier mobility depends on the electronic

structure of a given material, on whether the material is isotropic or anisotropic and on scattering mechanisms [22].

The Wiedemann-Franz law (Eq. (4)) provides an expression for κ_e in Eq. (3):

$$\kappa_e = \sigma LT = en\mu LT \tag{4}$$

where σ is the electrical conductivity, L the Lorenz number, T is the absolute temperature. For metals and degenerate semiconductors L assumes the Sommerfeld value of 2.44×10^{-8} W·Ω/K^2. For non-degenerate, single parabolic band materials, and acoustic phonon scattering conditions, L drops to 1.49×10^{-8} W·Ω/K^2 [23]. The Wiedemann-Franz law is based on the assumption that free electrons (an electron gas) transport heat and electricity in metals, for which the total thermal conductivity is approximately equal to κ_e. The value of the Lorenz number varies among materials and depends, e.g., on band structure, on the position of the Fermi level, and on temperature; for semiconductors L relates to the carrier concentration [24]. The Lorenz number can vary, particularly with carrier concentration, e.g., in low-carrier concentration materials it can be about 20% lower than for metals [25]. Important deviations from the Wiedemann-Franz law are seen, e.g., in multi-band materials [26, 27], in nanowires [28], in superconductors [29], and in the presence of disorder [30]. The latter will be important for the materials investigated here. κ and σ are always determined experimentally. An accurate determination of κ_e is critical, since κ_L is often calculated from the difference between κ and κ_e (Eq. (3)).

Electronic transport processes can be analyzed using the density functional theory (DFT), electronic band-structure calculations, and the Boltzmann transport theory [31–33]. The Fermi-Dirac distribution function can be included in the computations to deal with temperature effects. To get a more complete description of electron-transport or electron scattering in a solid material, the energy (ε) dependence of the relaxation time of electrons near the Fermi energy is needed. To calculate the σ (T), S (T), and $\kappa_e(T)$ the Boltzmann transport equation framework is applied.

A scattering mechanism includes scattering from charge carriers and phonons. Scattering from charge carriers includes ionized impurities, acoustic phonons, the phonon deformation potential and scattering at crystal boundaries. Phonon scattering consists of phonon–phonon-, point-defect- and phonon-carrier scattering. To calculate the total scattering rate as the sum of the individual contributions Eq. (5), Mathiessen's rule is used:

$$\frac{1}{\tau_{\text{total}}} = \sum \frac{1}{\tau_i} \tag{5}$$

where τ_i is the relaxation time for each scattering mechanism and τ_{total} is total relaxation time. Note that because (ε) is integrated in the Boltzmann framework, the temperature dependence of conductivity may not be the sum of the temperature dependence of simple scattering processes. For example, if scattering process A has a relaxation time of $\tau_A(\varepsilon)$ and scattering process B has a relaxation time of $\tau_B(\varepsilon)$, then the total ε dependence will be

$$\frac{1}{\tau_t(\varepsilon)} = \frac{1}{\tau_A(\varepsilon)} + \frac{1}{\tau_B(\varepsilon)} \tag{6}$$

$$\tau_t(\varepsilon) = \frac{\tau_A(\varepsilon) + \tau_B(\varepsilon)}{\tau_A(\varepsilon)\tau_B(\varepsilon)} \neq \tau_A(\varepsilon) + \tau_B(\varepsilon) \tag{7}$$

As shown in Eq. (7), the combination of two scattering mechanism is not simply a summation, unless other approximations apply.

Table 1 shows that many different scattering mechanisms have been published. Here, I provide a list of examples of scattering mechanisms of electrical-, and thermal conductivities, as well as the Seebeck coefficient for one case. T_F is the Fermi temperature, and T_{BG} is the Bloch-Grüneisen temperature.

Umklapp or inharmonic scattering is present in crystalline materials at high temperatures and is the scattering of phonons by other phonons in three-phonon resistive processes. The significance of the process increases as the temperature increases, i.e., when more phonons with larger wave vectors are excited [38].

Scattering mechanism	Temperature	κ or S	σ
Electron-Impurity Scattering [34]	$T \ll T_F$	$\kappa_e \propto T$	$\sigma \propto T^0$
Electron-Impurity Scattering [34]	$T \gg T_F$	$\kappa_e \propto T^{1/2}$	$\sigma \propto T^{-1/2}$
Electron–Phonon Scattering [34]	$T \ll T_{BG}$	$\kappa_e \propto T^{-2}$	$\sigma \propto T^{-5}$
Electron–Phonon Scattering [34]	$T_F \gg T \gg T_{BG}$	$\kappa_e \propto T^0$	$\sigma \propto T^{-1}$
Electron–Phonon Scattering [34]	$T \gg T_F$	$\kappa_e \propto T^{-1/2}$	$\sigma \propto T^{-3/2}$
Umklapp Scattering [35]	High T Low T	$\kappa_L \propto T^{-1}$ $\kappa_L \propto T$	—
Electron–Electron Scattering [36]	Low T	—	$\sigma \propto T^{-2}$
Mott Variable Range Hopping [37]	Low to high T	$S \propto T^{1/2}$	$\sigma \propto e^{-(T_0/T)^{1/4}}$
Efros-Shklovskii Variable Range Hopping [37]	Low to high T	—	$\sigma \propto e^{-(T_0/T)^{1/2}}$
Nearest Neighbor Hopping [37]	Low to high T	—	$\sigma \propto e^{-(T_0/T)^1}$

Table 1.
Scattering mechanism of electrical-, thermal conductivities, and Seebeck coefficient.

In many semiconductors that show 'glass-like' behavior, there is a change in the conduction mechanism with temperature from thermally activated to 'Variable Range Hopping' (VRH) conduction [39, 40]. According to Mott, electron hopping between nearest neighbor sites is not always favored at low temperatures as the sites may be significantly different in energy. It is possible that electrons prefer to move to an energetically similar but more remote site. In this regime, the following conduction law is expected for the variation of the conductivity of glass-like disordered systems [41, 42]:

$$\sigma = \sigma_0 e^{-(T_0/T)^\Upsilon} \tag{8}$$

where σ_0 is the pre-exponential factor, T_0 is a characteristic temperature. The condition $0 < \Upsilon < 1$ is fulfilled, if the VRH mechanism dominates the conduction. $\Upsilon = ¼$ corresponds to a Mott VRH, if the density of states around the Fermi level can be assumed to be constant; $\Upsilon = 1/2$ correlates with an Efros-Shklovskii VRH, if there is a gap at the Fermi level [41, 42]; $\Upsilon = 1$ agrees with a Nearest Neighbor Hopping (NNH) mechanism.

The most proper way to determine the accuracy of Υ in Eq. (8) is to analyze the electrical conductivity versus temperature by using the approach of Zabrodskii and Zinoveva [43] as follows. Let W be defined as

$$W(T) = \ln \left[\frac{d \ln \sigma(T)}{d \ln T} \right] \tag{9}$$

By inserting Eq. (8) into Eq. (9), $W(T)$ can be written as Eq. (10)

$$W(T) = \ln \Upsilon + \Upsilon \ln T_0 - \Upsilon \ln T \qquad (10)$$

$W(T)$ can also be used to determine metallic and insulating behavior. If the slope of $\ln [W(T)]$ vs. $\ln T$ is negative, the material is an insulator. However, if the slope is positive, the material behaves like a metal [37]. Generally, in semiconductors (doped or un-doped) $\sigma(T)$ and $S(T)$ have opposite temperature dependencies. In Mott's Variable Range Hopping the electrical conductivity depends on temperature as $\sigma \propto e^{-(1/T)^{1/(d+1)}}$ and the Seebeck coefficient as $S \propto T^{(d-1)/(d+1)}$, where d is the dimensionality of the system [44]. In our work, the system is 3D; $\sigma(T)$ and $S(T)$ vary with temperature as $\sigma \propto e^{-(1/T)^{1/4}}$ and $S \propto T^{1/2}$.

4. Selecting and making lead- and lead-yttrium ruthenates

Substitutions of atoms on the A- and/or B-site in pyrochlore, here $Pb_2Ru_2O_{6.5}$, change the thermoelectric properties. I have selected and synthesized two sets of ruthenate pyrochlore compounds, one with variable Pb:Ru ratio, the other constitutes solid solutions of Pb- and of Y-ruthenate (**Table 2**). Changing the Pb:Ru ratio changes A and B site occupancy and the defect concentrations. For example, reducing the number of Pb^{2+} ions creates more vacancies in the A_2O' sublattice and changes the properties of the already existing oxygen vacancies, which are occupied by Pb $6s^2$ electron lone-pairs in $Pb_2Ru_2O_{6.5}$. Less than two Pb^{2+} ions mean less electrons for the vacancies. Reducing Ru should affect electrical conductivity, which is mainly due to the RuO_6 backbone structure of ruthenate pyrochlores.

Compounds*	Stoichiometric variations
$Pb_{(2+x)}Ru_{(2-x)}O_{(6.5\pm z)}$	x: 0.0, −0.3, 0.3, 0.5, 0.7, 0.9; $0 \leq z \leq 0.5$
$Pb_{(2-x)}Ru_2O_{(6.5\pm z)}$	x: 0.2; $0 \leq z \leq 0.5$
$Pb_{(2-x)}Y_xRu_2O_{(6.5\pm z)}$	x: 0.0, 0.1, 0.2, 0.4, 1.0, 1.5, 2.0; $0 \leq z \leq 0.5$

*z was not measured; z = 0, known for $Pb_2Ru_2O_{6.5}$ and z = 0.5 for $Y_2Ru_2O_7$.

Table 2.
Lead ruthenate derivatives and lead yttrium ruthenate solid solutions.

Partial Pb-Y substitutions have been studied and showed a transition from metal-like electrical conductivity to semiconducting, prior to becoming an insulating material [45]. Since Pb in $Pb_2Ru_2O_{6.5}$ causes the width of the Ru t_{2g} block band to be fairly wide and that of yttrium to be narrower [13], then yttrium is an interesting element when expecting property changes for partial substitutions. Obviously, $^{VIII}Y^{3+}$ with its much smaller ionic radius than $^{VIII}Pb^{2+}$ reduces the Ru–O–Ru bond angle [13], thereby making the increasingly Y-rich compound less metallic.

The pyrochlores were made as follows. Equally sized powders, about 10 μm in size were cold pressed into pellets, reacted at high temperature (1173 K to >1273 K), crushed, pressed again into pellets, sintered, cooled, and then measured. Only $Pb_2Ru_2O_{6.5}$ and $Y_2Ru_2O_7$ have been studied by others. The electrical conductivity of $Pb_2Ru_2O_{6.5}$ has been measured frequently, as shown in **Table 3**.

The results depended on the method of synthesis and fluctuated between 120 ± 30 S/cm (298 K) [46] and 4651.2 S/cm (300 K) [6]. Temperatures higher than 598 K have also been studied [17, 47].

Reference*	Temp. range (K)	Synthesis	298-300 K	323 K	373 K	423 K	473 K	523 K	573 K
Tachibana et al. [6]	1 < T < 300	Single crystal	4651	—	—	—	—	—	—
Mayer-von Kürthy [7]	77 < T < 300	Solid state	2128	—	—	—	—	—	—
Takeda et al. [17]	298 < T < 1173	Solid state	631	513	479	447	417	389	251
Parrondo et al. [46]	298 < T < 598	Alkaline solution	120 ± 30	—	—	—	—	—	—
Song and Lee [47]	373 < T < 1073	Co-precipitation process	—	—	3490	3375	3250	3100	3150
Akhbarifar et al. [48]	298 < T < 598	Solid state	2137	2037	1902	1781	1702	1638	1579
Sleight [49]	4.2 < T < 298	Solid state	2000	—	—	—	—	—	—
Kobayashi et al. [50]	15 < T < 300	Solid state	1000	—	—	—	—	—	—

Except Perrondo et al., all authors measured σ(T) with DC 4-probe technique.

Table 3.
Known temperature dependences of electrical conductivity σ(T) of lead ruthenate.

5. Lead ruthenate derivatives

X-ray powder diffraction measurements and phase identification were performed. Search-match routines in *JADE9* software (Materials Data. Inc.) were used. The powder patterns were calibrated using a corundum (α-Al_2O_3) standard. X-ray powder diffraction patterns of lead ruthenate ($Pb_2Ru_2O_{6.5}$) and six derivatives are shown in **Figure 1**. All *d*-spacing and intensities match the isometric pyrochlore crystal structure. Lattice constants a_0 were calculated for all samples. The lattice constant of pure lead ruthenate (a_0 = 1.0257 nm) was in good agreement
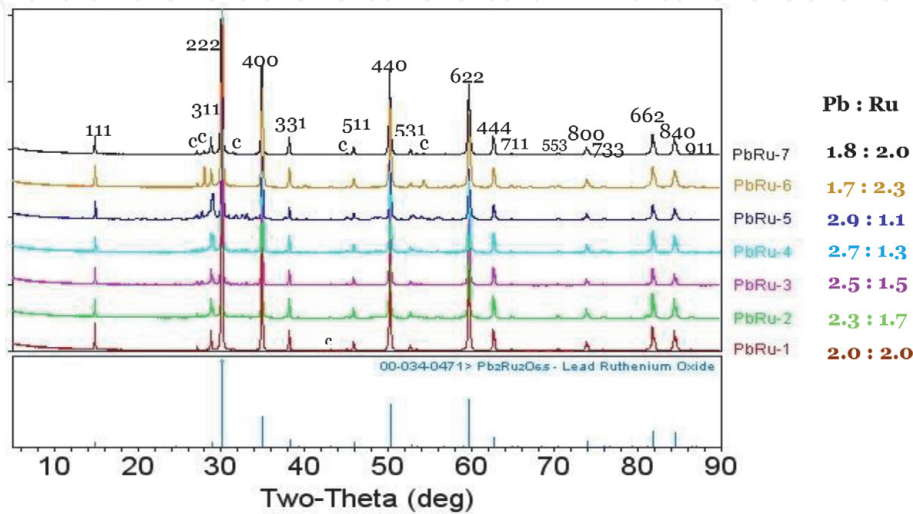

Figure 1.
X-ray diffraction patterns of lead ruthenate pyrochlore [51] and six derivatives (below: Reference pattern 00-034-0471 of $Pb_2Ru_2O_{6.5}$; 'c' = unidentified contaminant).
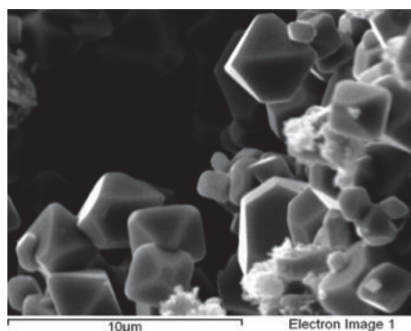
Figure 2.
SEM image showing octahedral crystals of our $Pb_2Ru_2O_{6.5}$.

with Jade reference # 00-034-0471 by Horowitz et al. [52] with a value of 1.0252 nm.

Substitutions affect a_0, but the isometric unit cell is maintained in all cases. A closer look at the X-ray spectra at $2\theta = 28°$ showed that traces of unreacted RuO_2 may be present, particularly in Pb:Ru = 1.7:2.3. The yield of all synthesized pyrochlores is close to 100%.

Solid-state synthesis of pyrochlores involved a series of manipulations, which introduced ZrO_2 from milling containers, SiO_2 and Al_2O_3 from glass mortars and pestles. The impurities were analyzed by semi-quantitative X-ray fluorescence and amounted to $\approx$ 1 wt.%. When present, unreacted RuO_2 amounted to $\approx$ 1 wt.% as well. Suggesting an overall purity of our pyrochlores of at least 98 wt.%. **Figure 2** shows a secondary electron image of octahedral $Pb_2Ru_2O_{6.5}$ crystals.

5.1 Electrical- and thermal conductivity and Seebeck coefficients of lead ruthenate derivatives

In this section I present and discuss thermoelectric properties of derivatives of lead ruthenate ($Pb_{(2+x)}Ru_{(2-x)}O_{(6.5\pm z)}$ and $Pb_{(2-x)}Ru_2O_{(6.5\pm z)}$), **Table 2**). Comparisons are made with the published results of lead ruthenate [48].

Figure 3a shows electrical conductivity as a function of temperature for lead ruthenate derivatives. All conductivities decrease with increasing temperature, suggesting metal-like performance of all ceramics. The lead ruthenate derivative with a deficiency of lead, i.e., $Pb_{1.8}Ru_2O_{6.5\pm z}$ exhibits the highest electrical conductivity. The lowest conductivity was seen for the derivative with an excess of lead and a deficiency of ruthenium, i.e., $Pb_{2.9}Ru_{1.1}O_{6.5\pm z}$. The oxygen content of the derivatives was not measured.
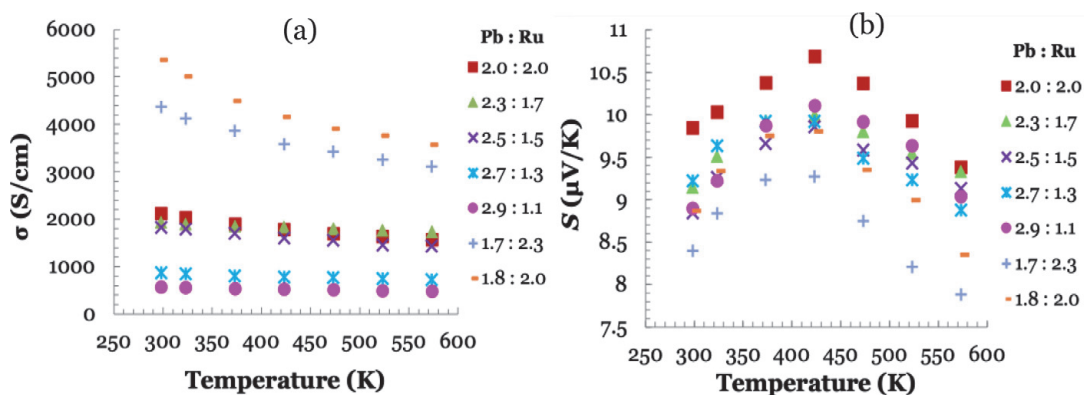

Figure 3.
(a) Electrical conductivity and (b) Seebeck coefficients of lead ruthenate derivatives.

Electrical conductivity is attributed essentially to transport of electrons in and through BO_6 octahedra, the backbone of the pyrochlore structure [53, 54]. The Pb $6s^2$ electron lone-pair is highly localized in defect pyrochlores like lead ruthenate with oxygen deficiency (O′ vacancies) in the sublattice. Hence, the electron lone-pair is stereo-chemically active. This results in the formation of ordered oxygen vacancies and the displacement of Pb closer to the vacancy [14]. In this way, the pyrochlore structure is stabilized vis-à-vis the perovskite structure [18]. Pb may be present in lead ruthenates in two valence states as $Pb^{2+}_{1.5}Ru^{4+}_2Pb^{4+}_{0.5}O_{6.5}$ [9]. Alternatively, Ru could be present in two valence states as Ru^{4+} and Ru^{5+}, i.e., $Pb_2Ru^{4+}_{1.0}Ru^{5+}_{1.0}O_{6.5}$. Even with some Pb^{4+} present, the pyrochlore structure would still be sufficiently stabilized by the Pb^{2+} $6s^2$ electron lone-pair.

Removal of Ru, i.e., decreasing the overlap of the Pb $6p$ with the Ru $4d$ bond, should result in a decreasing electrical conductivity, relative to pure lead ruthenate, which is confirmed by the experimental results (B-site stoichiometry <2). For charge balance reasons, it is assumed that Pb enters the B-site as Pb^{4+}, which also means absence of some Pb $6p$ electrons. Decreasing Pb^{2+} on the A-sites (x = 1.7) without substitutions increased the electrical conductivity significantly, which may be the result of creating more oxygen vacancies and vacancies in the $A_2O′$ sublattice. The relatively strong increase of electrical conductivity due to increasing Ru to 2.3 at the expense of Pb to 1.7 is less easy to explain. The replacement of 2 Pb^{2+} by one Ru^{4+} on the A site would cause an A-site vacancy, which could increase electrical conductivity. Ru^{4+} is smaller than Pb^{2+}. This should cause rattling of Ru, which would increase phonon scattering and thus decrease thermal conductivity. This will be discussed further in context with thermal conductivity and scattering mechanisms.

Figure 3b shows that the Seebeck coefficients go through a maximum near 423 K for all lead ruthenate derivatives. The dependence of the Seebeck effect on the composition of these pyrochlores is not very pronounced. The highest and lowest coefficients deviate from each other by about 15%, independent of temperature. A surprising finding was that $S(T)$ increased initially with increasing temperature and then decreased with further increasing temperature. Since $S(T)$ is positive the majority of charge carriers are holes, i.e., lead ruthenate pyrochlore and its derivatives exhibit p-type conductivity. The kind of temperature dependence of S found for these pyrochlores has been observed in other systems as well. For example, $Y_{2-x}Bi_xRu_2O_7$ show a broad maximum at 170 K for x = 1.6 [9], but the authors gave no explanation. Paschen [51] observed a maximum of $S(T)$ in a clathrate-like material, i.e., in $Eu_3Pd_{20}Ge_6$, at about 120 K. The author attributed the maximum to valence fluctuations of Eu (3^+ and 4^+). Sidharth et al. [55] measured a broad maximum of $S(T)$ for tin chalcogenides, $SnSe_{1-x}Te_x$ between 400 K and 600 K. These authors discuss their findings in terms of the influence of carrier-phonon-, carrier-carrier scattering and conductivity-limiting bipolar conduction at high temperature. Tse et al. [56] reported a maximum of S for Na_xSi_{46} clathrates at x = 16 for 200 K. Certain clathrates are metallic, but their thermal conductivity resembles that of glass-like solids, as with lead ruthenate [48] and the derivatives studied here. Tse et al. [56] ascribed the trend of $S(T)$ as a function of sodium content to the band profile of the silicon framework. The rise of $S(T)$ with increasing temperature to a maximum and the decrease with further increasing temperature was qualitatively reproduced by raising the Fermi level. A maximum in the temperature dependence of $S(T)$ was also seen in bismuth metal thin films. For a 33 nm thick film, the maximum occurred near 425 K [57]. The authors of [57] discussed the phenomenon by taking into account the temperature dependence of the Fermi energy, which cannot be neglected because bismuth has a low Fermi energy. Hence, increasing and decreasing Seebeck coefficients have been observed

in a variety of materials and in different temperature ranges. Explanations of respective data for different materials vary.

The Seebeck coefficient of these *p*-type pyrochlores is inversely proportional to the carrier concentration (Eq. (2)). Before the onset of intra-band minority carrier (electron) excitation at lower temperatures, $S(T)$ increases with T (**Figure 3b**), confirming metallic behavior of all pyrochlores. At higher temperatures the Fermi distribution broadens, which leads to an exponential increase in minority electrons, due to thermal excitation and resulting in a reduction of the Seebeck coefficient [58]. The Seebeck coefficient reaches a maximum, in this case at 423 K (**Figure 3b**) for all derivatives.

Figure 4 shows the results of thermal conductivity measurements of all lead ruthenate pyrochlores. Thermal conductivity increases with temperature and was found to have increased in all derivatives above that of lead ruthenate. Note that the compounds 1.7:2.3 and 1.8:2.0 showed the highest electrical conductivities (**Figure 3a**), while their thermal conductivities are least affected (**Figure 4**). This will be addressed in the next section. I noticed an increase of the total thermal conductivity with temperature in the crystalline lead ruthenate and its derivatives, which is typical of glass-like materials. A glass-like behavior of all these pyrochlores is likely due to an electronic contribution from an increasing concentration of minority electrons with temperature, which also contributed to the downturn of the Seebeck coefficients.

The presence of structural defects and a large unit cell create pronounced anharmonicity, which lowers the thermal conductivity [59]. $Pb_2Ru_2O_{6.5}$ possesses intrinsic disorder characteristics, i.e., vacancies in the A_2O' sublattice and stereo-chemically active $6s^2$ electron lone-pairs on Pb. Similar defects can be expected to prevail in our derivatives. These defects cause a glass-like temperature dependence of thermal conductivity of our lead ruthenate derivatives. This was also observed, e.g., in chalcogenides, clathrates, and yttrium-stabilized zirconia (YSZ) [38], and materials with intrinsic disorder [60–63]. The thermal conductivity of lead ruthenate is close to that of vitreous silica [48], which is 1.93 W/m·K at 373 K. With increasing temperature, the 3-phonon resistive process (Umklapp scattering) and excitation of more phonons with larger wave vectors become increasingly important [64], thereby lowering the lattice thermal conductivity of a crystal [59].
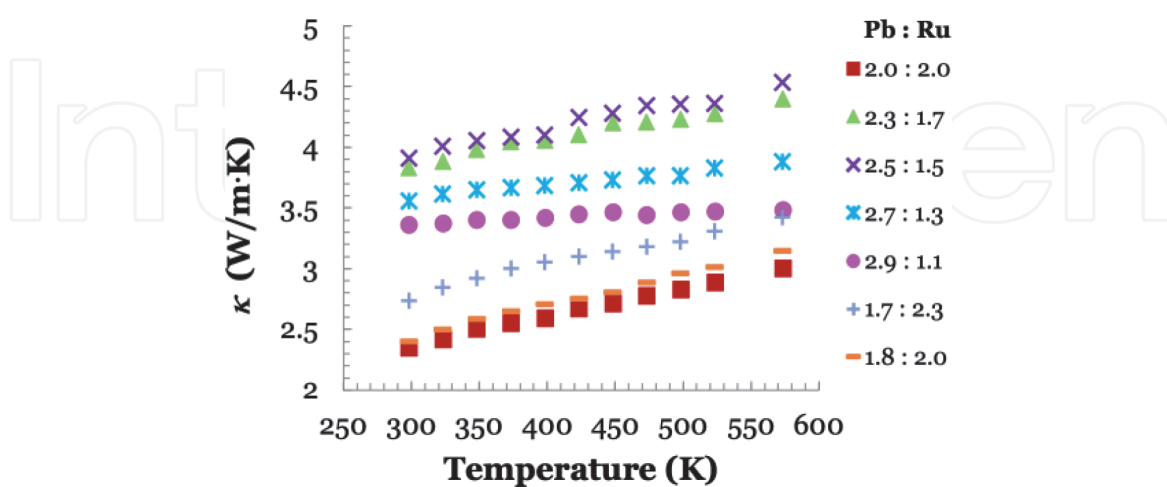

Figure 4.
Thermal conductivity of lead ruthenate derivatives.

5.2 Scattering mechanisms in lead ruthenate derivatives

The measured thermal conductivity κ is the sum of electronic κ_e and lattice thermal conductivity κ_L (Eq. (3)). The electronic and lattice contributions are

plotted in **Figure 5a** and **b**, respectively. The electronic thermal conductivity increased with temperature and decreased with increasing Pb content. The Pb: Ru = 1.8:2.0 and the Pb:Ru = 1.7:2.3 pyrochlores, respectively, have the highest electronic thermal conductivities. With one exception, the lattice thermal conductivities are almost independent of temperature but vary with composition. Partial removal of Pb from $Pb_2Ru_2O_{6.5}$ lowers the lattice thermal conductivity. Using the Lorenz number of 2.44×10^{-8} WΩ/K^2 for metals to calculate κ_e yielded negative values for κ_L, which is meaningless. To avoid this, I used 1.49×10^{-8} WΩ/K^2, which has been applied for non-degenerate, single parabolic band materials, and acoustic phonon scattering conditions [62].

As expected from electrical conductivities (**Figure 3a**), the compounds with a lead deficiency show κ_e values higher than in pure lead ruthenate (**Figure 5b**). However, the κ_L values are the lowest of all. These compounds are presumably the ones with the highest defect concentrations of all lead ruthenate derivatives, which are assumed to increase phonon scattering and thus lower κ_L.
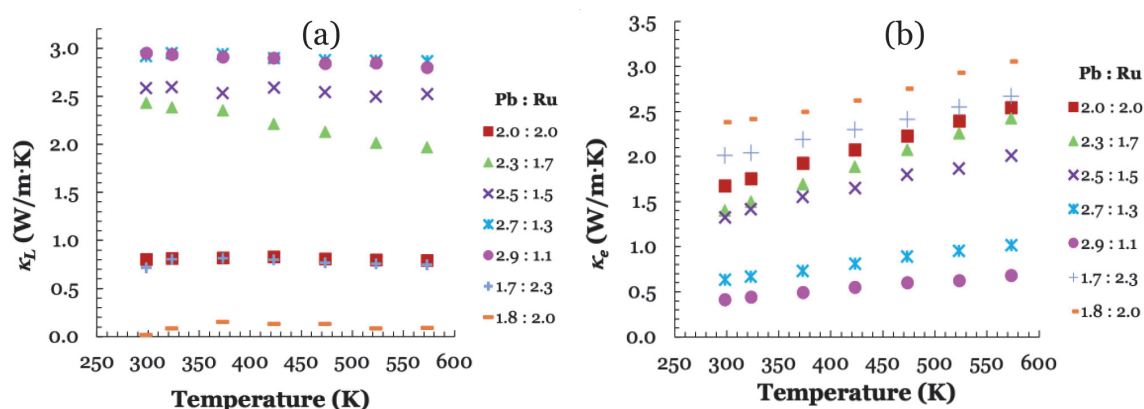

Figure 5.
(a) Lattice- and (b) electronic thermal conductivity of lead ruthenate derivatives.

The electrical and thermal conductivity data of lead ruthenate derivatives have been analyzed for underlying scattering mechanisms. The temperature dependence of the scattering mechanisms listed in **Table 1** were least-squares-fitted to the experimental data. The goodness of the fits was analyzed by using the reduced chi-squared statistic (χ^2/DOF) (Eq. (11)) and the best fit was assumed to have identified the most likely scattering process.

$$\chi^2/DOF = \frac{Sum\ of\ squared\ errors}{DOF} \tag{11}$$

where DOF is the number of degrees of freedom, which is the number of data points minus the number of fit parameters. For all seven synthesized pyrochlores, the best fits for $\sigma(T)$, $\kappa_e(T)$, and $\kappa_L(T)$ were $T^{-1/2}, T^{1/2}$, and T^{-1}, respectively. All fits for all pyrochlores pointed at the same underlying scattering mechanisms. A graphical representation of these dependencies can be found in [48] for pure lead ruthenate. According to **Table 1**, the underlying scattering mechanism is 'electron impurity scattering'. Since this mechanism prevails only at $T \gg T_F$ (**Table 1**), the excellent match between data and the fits suggests that the Fermi temperature T_F of lead ruthenate and its derivatives is below room temperature. Other joint scaling shapes rule out other combinations of dominant scattering mechanisms. This is evidence that traditional electron-acoustic phonon scattering is suppressed and thus most scattering is due to intrinsic disorder and impurities.

The lattice thermal conductivity $\kappa_L(T)$ of lead ruthenate and all derivatives varies with T^{-1}. This dependence suggests that the 3-phonon resistive process

(Umklapp scattering, **Table 1**) is responsible for the decrease of $\kappa_L(T)$ in all compositions. This finding supports the electron-impurity scattering mechanism for $\sigma(T)$ and $\kappa_e(T)$ (**Table 1**) [64], because transport properties are sensitive to structural disorder such as site substitutions, vacancies and localized impurities, all of which are present in these pyrochlores at different concentrations. These defects can lower the thermal conductivity to glass-like behavior [59]. In this regard, compounds with stereochemically active electron lone-pairs associated with constituent atoms (here Pb^{2+} on the pyrochlores' A-site) have attracted significant attention. Other examples are Cu_3SbSe_3, Ag_5bSe_2, and other chalcogenides. The 3-phonon resistive process will be addressed again in Section 6.2. The same causes as here hold there for Umklapp scattering for lead-yttrium ruthenate solid solutions. The electronic contribution $\kappa_e(T)$ to the total thermal conductivity $\kappa(T)$ increased with increasing temperature and was estimated to be about 72% at 25°C and 85% at 300°C, respectively. The total thermal conductivity $\kappa(T)$ results mainly from electronic thermal conductivity.

6. Lead yttrium ruthenate solid solutions

We have reported recently [45] on electrical conductivity and Seebeck coefficients of lead yttrium ruthenate solid solutions. The focus of that investigation was on finding and explaining a metal insulator transition in a suite of Pb-Y ruthenate solid solutions between the metal-like paramagnetic $Pb_2Ru_2O_{6.5}$ and the antiferromagnetic Mott insulator $Y_2Ru_2O_7$. Only 10 mol% of Pb needed to be replaced by yttrium to reach the point of transition from a metal-like to a semiconducting ceramic. Following the Mott-Hubbard model, yttrium opens the Mott-Hubbard gap and fills the lower Mott-Hubbard band with localized t_{2g} electrons thereby changing the mechanism of electron transport [45].

In this section I report on the hitherto unknown thermal properties of lead yttrium ruthenates and analyze these together with our previously published measurements on electrical conductivity and the Seebeck effect [45] in terms of quantum-physical scattering.

Structure and purity of all samples (**Table 2**) have been determined by X-ray diffraction and X-ray fluorescence analysis, respectively. The X-ray diffraction patterns of pure lead and yttrium ruthenate are known (Jade reference # 00-034-0471, a_0 = 1.0252 nm and # 00-028-1456, a_0 = 1.0139 nm, respectively). The solid solutions are all of isomeric structure and follow Vegard's law, i.e., the unit cell parameter decreases linearly with increasing concentration of Y^{3+} (r = 0.1019 nm), which is smaller than Pb^{2+} (r = 0.129 nm) [45].

6.1 Thermal conductivity of lead yttrium ruthenate solid solutions

The results of thermal conductivity measurements are shown in **Figure 6**. Thermal conductivity κ increases with temperature. Pure lead ruthenate has the highest thermal conductivity (2.35 W/m·K) of the pyrochlores at all temperatures [48]. As the Y concentration increases, κ and its temperature dependence decrease. Pure yttrium ruthenate has the lowest thermal conductivity.

κ increases with temperature up to an yttrium concentration of x = 1.0. At and above x = 1.5, κ is very low and nearly temperature independent. These pyrochlores are insulators as indicated by low electrical conductivity as well [45]. The increase of κ with increasing T, and the low values of κ are typical of glass-like behavior, although all these pyrochlores are crystalline. As with lead ruthenate derivatives, glass-like behavior is probably due to a contribution to κ_e of an increasing

concentration of minority electrons with increasing temperature, which also contributed to the decrease of the Seebeck coefficient for x = 0 to 1.5 [45].
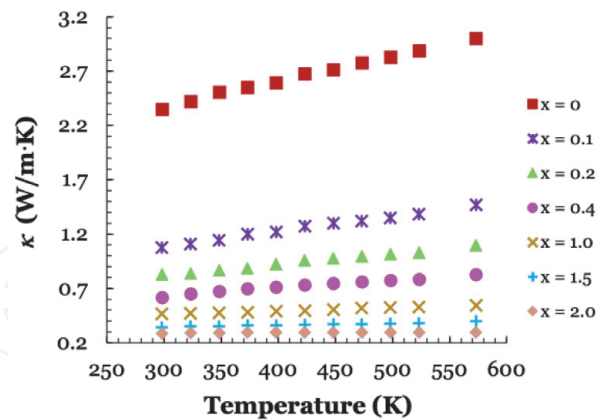

Figure 6.
Thermal conductivity of Pb- and Y-ruthenate and solid solutions.

6.2 Scattering mechanisms in lead yttrium ruthenate solid solutions

The electronic thermal conductivity κ_e was calculated with Eq. (4), the lattice thermal conductivity κ_L with Eq. (3) and plots are shown in **Figure 7a** and **b**.

The electronic thermal conductivity κ_e (**Figure 7a**) decreases with increasing Y content but increases with temperature. The slope of the temperature dependence of κ_e decreases with increasing concentration of yttrium. **Figure 7a** (lower diagram) contains the data for the two insulators $Pb_{(2-x)}Y_xRu_2O_{(6.5+z)}$ with x = 1.5 and 2.0 on a different scale, to show that there is still a temperature dependence of κ_e. $Y_2Ru_2O_7$ shows the lowest electronic thermal conductivity.

The lattice thermal conductivity κ_L decreases with increasing temperature for $x \leq 0.2$ (**Figure 7b**). Between x = 0.4 and x = 2.0 κ_L becomes temperature independent. κ_L increases initially with temperature in pure lead ruthenate (x = 0).

In this section electrical- and thermal conductivity and Seebeck coefficients of the pyrochlores $Pb_{(2-x)}Y_xRu_2O_{(6.5+z)}$ ($0 \leq x \leq 2$, $0 \leq z \leq 0.5$) will be analyzed for the underlying scattering mechanisms. To do so, the temperature dependence of the scattering mechanisms listed in **Table 1** were fitted to the experimental data. The goodness of all fits was analyzed by using Eq. (11), which yielded the most likely scattering mechanisms.
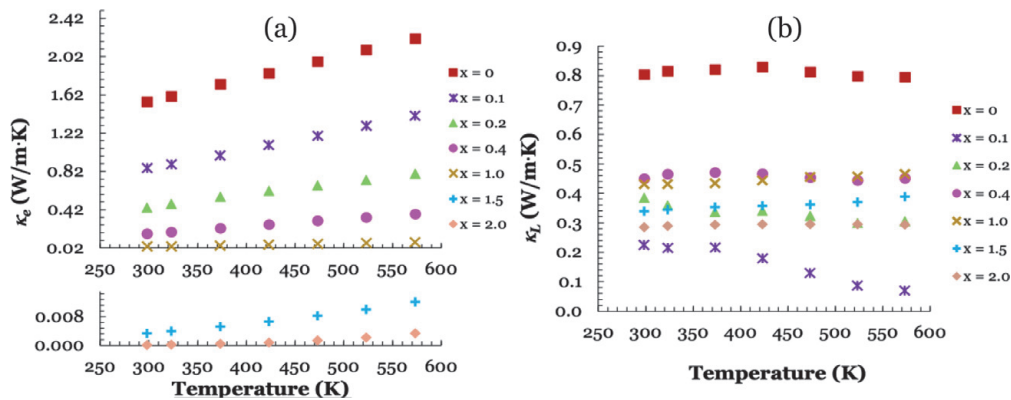

Figure 7.
(a) Electronic- and (b) lattice thermal conductivity of Pb- and Y-ruthenate and solid solutions.

As shown in **Table 1**, for most scattering mechanisms at least two properties, for example, $\sigma(T)$ and $\kappa_e(T)$ must be fitted together to show the respective temperature dependencies. For $Pb_{(2-x)}Y_xRu_2O_{(6.5+z)}$ with x = 0 and 0.1 the best fits of electrical conductivity data $\sigma(T)$ and of the electronic component of thermal conductivity $\kappa_e(T)$ vary with $T^{-1/2}$ and $T^{1/2}$, respectively (see **Figure 8a** and **b**). According to **Table 1** the underlying scattering mechanism is 'electron-impurity scattering' at $T \gg T_F$ [37]. The lattice thermal conductivity $\kappa_L(T)$ varies with T^{-1} suggesting that the 3-phonon resistive process (Umklapp scattering, **Table 1**) is responsible for the decrease of $\kappa_L(T)$ in the pyrochlores with x = 0 and x = 0.1 moles of yttrium. This finding supports the electron-impurity scattering mechanism for $\sigma(T)$ and $\kappa_e(T)$ (**Table 1**) [41]. The experimental data and the least squares fits are shown in **Figure 8a–c**.

For $Pb_{(2-x)}Y_xRu_2O_{(6.5+z)}$ with x = 0.2 and x = 0.4 the best fits of the electrical conductivity data $\sigma(T)$ and of the electronic component of thermal conductivity $\kappa_e(T)$ did not allow for an unambiguous determination of the scattering mechanism. The goodness of two fits was practically identical. Two variations of $\sigma(T)$ and $\kappa_e(T)$ with temperature are equally likely: $\sigma(T)$ varies with $T^{-1/2}$ or with T^{-1} and $\kappa_e(T)$ varies with $T^{1/2}$ or with T^0. Based on **Table 1** the underlying scattering mechanisms are 'electron-impurity scattering' at $T \ll T_F$ provided that $\sigma(T)$ varies with $T^{-1/2}$ and $\kappa_e(T)$ with $T^{1/2}$. If $\sigma(T)$ varies with T^{-1} and $\kappa_e(T)$ with T^0 then 'electron–phonon scattering' at $T_{BG} \ll T \ll T_F$, is the mechanism (**Table 1**) [37]. The lattice thermal conductivity $\kappa_L(T)$ varies with T^{-1} implying Umklapp scattering and supports the electron-impurity scattering mechanism. The actual scattering process could also be a combination of the two afore-mentioned mechanisms for which the temperature dependence would be unknown. In principle, more information could be obtained from an evaluation of Eq. (5), which has not been done yet. The fits for x = 0.4 are the electron-impurity scattering as shown in **Figure 8**. **Figure 8a–c** show
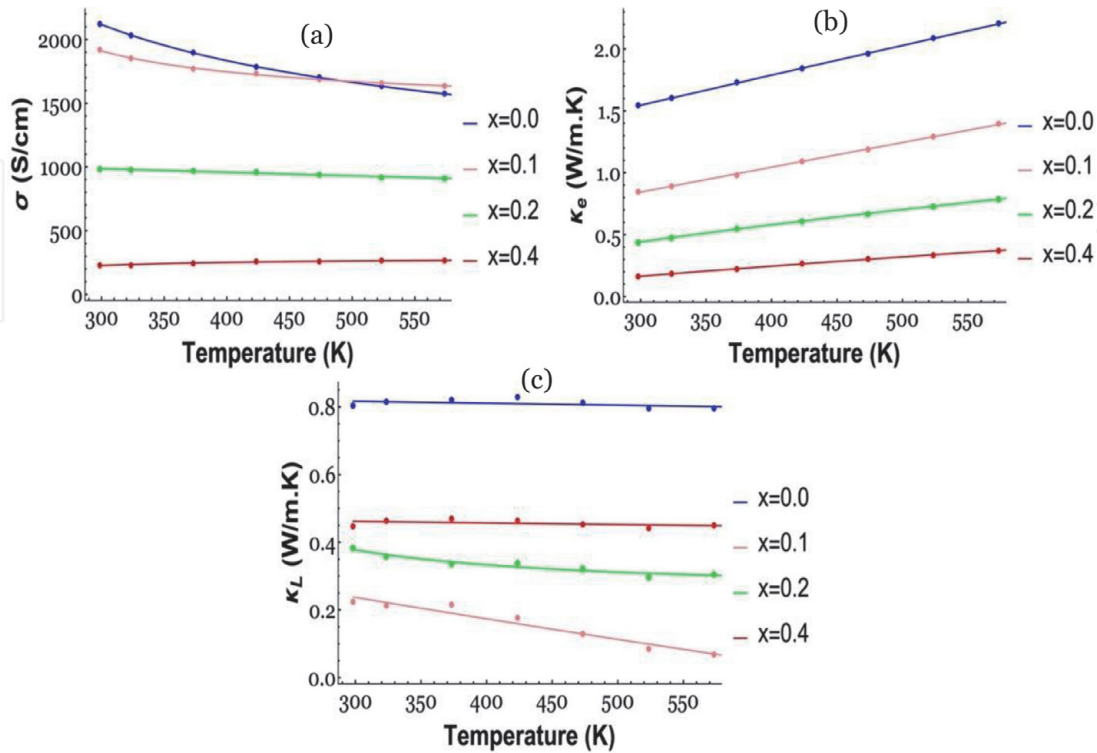

Figure 8.
Measured (a) electrical conductivity, (b) electronic-, and (c) lattice thermal conductivity fits as a function of T for $Pb_{(2-x)}Y_xRu_2O_{(6.5+z)}$ with x = 0, 0.1, 0.2, and 0.4 moles of Y.

$Pb_{(2-x)}Y_xRu_2O_{(6.5+z)}$ with x = 0, 0.1, 0.2, and 0.4 fitted with $T^{-1/2}, T^{1/2}$, and T^{-1} for σ, κ_e, and κ_L, respectively.

For $Pb_{(2-x)}Y_xRu_2O_{(6.5+z)}$ with x = 1.0 a clear selection of a mechanism cannot be made. The selection criteria, i.e., best least squares fit and goodness of the fit, allow for three scattering mechanisms. $\sigma(T)$ could vary with $T^{-1/2}$ and $\kappa_e(T)$ with $T^{1/2}$ or $\sigma(T)$ varies with T^{-1} and $\kappa_e(T)$ with T^0. Based on **Table 1** the underlying scattering mechanism would be electron-impurity scattering at $T \ll T_F$ or electron–phonon scattering at $T_{BG} \ll T \ll T_F$, or both (**Table 1**) [34]. The lattice thermal conductivity $\kappa_L(T)$ varies with T^{-1} implying Umklapp scattering and supports the electron-impurity scattering mechanism. The third possibility is that the Mott Variable Range Hopping (MVRH) mechanism [20] is active, which requires a $T^{1/2}$ dependence of $S(T)$ and for $\sigma(T)$ an $\exp(-1/T)^{1/4}$ dependence. Fitting $T^{1/2}$ to $S(T)$ yielded a satisfactory goodness of the fit. The same was the case when fitting the exponential function to the $\sigma(T)$ data. As I mentioned for x = 0.2 and 0.4, here with an yttrium content of 1.0 mole there could be a combination of the scattering mechanisms for which the temperature dependence could be determined using Eq. (5). This pyrochlore, like the ones in the previous section are in the MIT zone. This explains why there may be more than one scattering process active. The MVRH fitting is shown in **Figure 9**.

For $Pb_{(2-x)}Y_xRu_2O_{(6.5+z)}$ with x = 1.5 and 2.0 the best fits of electrical conductivity $\sigma(T)$ varies with $\exp(-1/T)^{1/4}$ and the Seebeck coefficients with $T^{1/2}$. As for x = 1.0, MVRH can be suggested. Mott's variable range hopping model describes hopping conduction between localized states with electron energies close to the Fermi level [41, 65, 66]. Hopping takes into account both thermally activated hopping over an energy threshold and phonon-assisted tunneling between localized states. For thermally activated hopping the Boltzmann factor $\exp(-W/k_BT)$ applies, where W is the energy barrier between the localized states. The electrical conductivity of the pyrochlores on the insulator side of the MIT shows thermally activated conduction characteristics (Figure 3 in [45]). This behavior indicates transport by the MVRH [67]. It could be due to a random potential caused by yttrium substitution [9]. **Figure 9** shows fitting of $Pb_{(2-x)}Y_xRu_2O_{(6.5+z)}$ with x = 1.0, 1.5, 2.0 by MVRH for σ and S.

The figure of merit zT of a thermoelectric material determines its value for practical applications. Respective values have been calculated for lead ruthenate derivatives and for Pb-Y ruthenate solid solutions. All zT values are still more than two orders of magnitude below those achievable today with other ceramics. The highest zT for all pyrochlores studied here was 7.3×10^{-3} at 523 K for $Pb_{1.9}Y_{0.1}RuO_{6.5\pm z}$. Since the focus of this work was on quantum physical

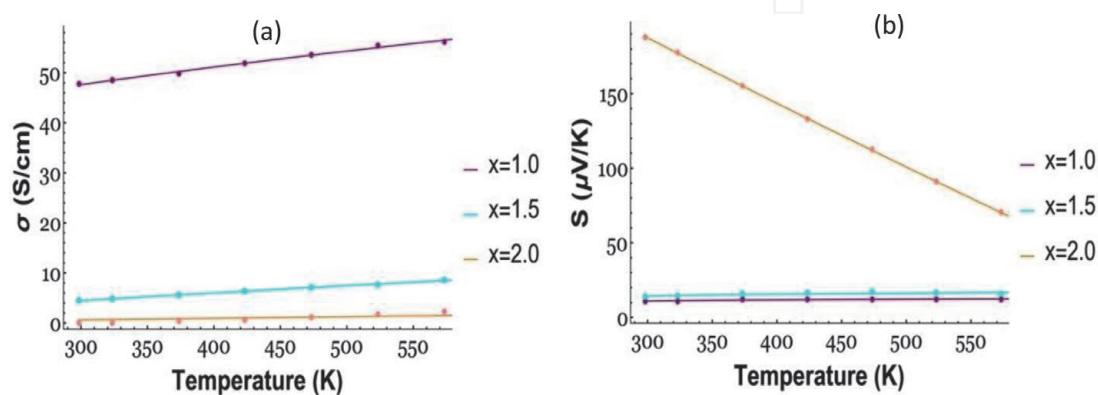**Figure 9.**
Measured electrical conductivity (a) and Seebeck coefficients (b) with respective fits as a function of temperature for $Pb_{(2-x)}Y_xRu_2O_{(6.5+z)}$ with x = 1.0, 1.5, and 2.0.

interpretation of the pyrochlores' thermoelectric properties, no effort was made yet to search for pyrochlores with higher figures of merit.

7. Summary and conclusions

Thermoelectric properties of ceramics are determined by their crystal structure and chemical composition. Important structural details affecting the transport mechanisms of heat and electricity are, e.g., vacancies, impurities, lattice site occupancy, lone pair electrons, and substitutions. The nature of these structural details can determine or change scattering mechanisms that determine the thermoelectric performance of the material. A selection of published mechanisms has been compiled. The way of testing these mechanisms by fitting respective mathematical functions to experimental data and the quantitative evaluation of the fits have been shown in this chapter, based on a large number of experimental data.

All thermoelectric properties of isomorphic lead ruthenate pyrochlores (defect pyrochlores) with different Pb:Ru atom ratios were measured and analyzed in quantum-physical terms to interpret transport mechanisms of thermal and electrical conductivity and to understand the temperature dependence of the Seebeck effect. All seven pyrochlores were p-type, exhibiting common features such as site substitutions, vacancies and some impurities, to which transport mechanisms are sensitive. Therefore, the same scattering mechanisms were seen for all pyrochlores, specifically, electrical conductivity $\sigma(T)$, which varied with $T^{-1/2}$, the electronic part of thermal conductivity $\kappa_e(T)$ varied with $T^{1/2}$ and the lattice thermal conductivity $\kappa_L(T)$ with T^{-1}. Hence, $\sigma(T)$ and $\kappa_e(T)$ were governed by electron-impurity scattering and $\kappa_L(T)$ by the 3-phonon resistive process (Umklapp scattering), which supports the electron-impurity scattering mechanism. The Seebeck effect was inversely proportional to the carrier concentration.

Measurements and quantum-physical analyses were also done with lead-yttrium ruthenate solid solutions, which are defect pyrochlores as well. The temperature dependence of the Seebeck coefficient was qualitatively the same as for the lead ruthenate and derivatives. The same interpretation applies. A metal–insulator transition (MIT) occurred, if 0.2 moles of Pb were replaced by Y. The endmember $Pb_2Ru_2O_{6.5}$ shows metal-like behavior. $Y_2Ru_2O_7$ is an insulator. Impurity scattering prevailed until the MIT was reached. The temperature functions of electrical conductivity and electronic thermal conductivity were the same as for the lead ruthenates. On the semiconductor/insulator side of the MIT, up to about one mole of yttrium, several scattering processes were equally likely, e.g., electron-impurity- and electron–phonon scattering. From one to two moles of yttrium, the Mott-Variable-Range Hopping mechanism was active, as suggested by $\sigma(T)$ varying with $\exp(-1/T)^{1/4}$. All figures of merit zT were small, about 7.3×10^{-3} maximum at 523 K.

Based on these findings the following conclusions are provided:

- In previous work, glass-like thermal conductivity of $Pb_2Ru_2O_{6.5}$ was found. The same was the case here for lead ruthenate derivatives (Pb:Ru variations). Obviously, an increasing concentration of minority electrons with temperature, a likely explanation of glass-like behavior, is not significantly affected by the rather large changes of the pyrochlore stoichiometry and site occupation. Thermal conductivity increased at maximum only by a factor of less than two.

- Significant changes of electrical conductivity were seen and can be related to site occupancy and ion valence.

- Seebeck coefficients of $Pb_2Ru_2O_{6.5}$ increased slightly with temperature and decreased after a maximum at 423 K. A remarkable insensitivity of this temperature dependence vis-à-vis Pb:Ru changes was noticed, suggesting that the underlying temperature dependence of the concentration of minority electrons is little affected by Pb:Ru concentration changes.

- Mathematical analyses of the measured thermoelectric properties pointed at the same underlying scattering mechanisms in all compounds, mainly a result of structural defects, not of the Pb:Ru ratio.

- Introducing yttrium into the metal-like $Pb_2Ru_2O_{6.5}$ changes the thermoelectric properties more drastically than variations of the Pb:Ru ratio.

- Scattering mechanisms were affected by the metal–insulator transition (MIT). Changes of bond angles, bond distances, and electronic structures (Mott-Hubbard) at the MIT are likely to affect heat- and electricity transport, which was reflected by the finding that different scattering mechanisms were active on either side of the MIT.

- Knowledge of scattering mechanisms and their relation to structural details and composition can provide guidance to tailor and optimize thermoelectric properties of a material.

Acknowledgements

Conflict of interest

The author does not have any conflict of interest.

Author details

Sepideh Akhbarifar
The Catholic University of America, Vitreous State Labratory, Washington D.C.,
USA

*Address all correspondence to: sepideha@vsl.cua.edu

IntechOpen

References

[1] Terasaki I, Sasago Y, Uchinokura K. Large thermoelectric power in $NaCo_2O_4$ single crystals. Physical Review B. 1997; 56:R12685–R12687

[2] Chakoumakos B.C. Systematics of the pyrochlore structure type, ideal $A_2B_2X_6Y$. Journal of Solid State Chemistry. 1984; 53:120-129

[3] Chakoumakos B.C. Pyrochlore, McGraw-Hill Yearbook of Science & Technology 1987, edited by S.P. Parker, McGraw-Hill, Inc., New York; 1986. p. 393

[4] Subramanian M.A, Aravamudan G, Subba Rao G.V. Oxide pyrochlore–A review. Solid State Chemistry. 1983; 15: 55-143

[5] Sleight A.W, Bouchard R.J. National Bureau of Standards Special Publication 364, Solid State Chemistry, Proceedings, 5th Materials Research Symposium; 1972. p. 227

[6] Tachibana M, Kohama Y, Shimoyama T, Harada A, Taniyama T, Itoh M, Kawaji H, Atake T. Electronic properties of the metallic pyrochlore ruthenates $Pb_2Ru_2O_{6.5}$ and $Bi_2Ru_2O_7$. Physical Review B. 2006; 73:193107

[7] Mayer-von Kürthy G, Wischiert W, Kiemel R, Kemmler-Sack S. System $Bi_{2-x}Pb_xPt_{2-x}Ru_xO_{7-z}$: A pyrochlore series with a metal-insulator transition. Journal of Solid State Chemistry. 1989; 79:34-45

[8] Bouchard R.J, Gillson J.L. A new family of bismuth precious metal pyrochlores. Material Research Bulletin. 1971; 6:669-680

[9] Yoshii S, Sato M. Studies on Metal-Insulator transition of pyrochlore compound $Y_{2-x}Bi_xRu_2O_7$. Journal of the Physical Society of Japan. 1999; 68: 3034-3040

[10] Klein W, Kremer R.K, Jansen M. $Hg_2Ru_2O_7$, a new pyrochlore showing a metal-insulator transition. Journal of Materials Chemistry, 2007; 17: 1356-1360

[11] Takeda T, Nagata M, Kobayashi H, Kanno R, Kawamoto Y, Takano M, Kamiyama T, Izumi F, Sleight A.W. High-Pressure Synthesis, Crystal Structure, and Metal-Semiconductor Transitions in the $Tl_2Ru_2O_{7-\delta}$ Pyrochlore. Journal of Solid State Chemistry. 1998; 140:182-193

[12] Lee S, Park J.G, Adroja D.T, Khomskii D, Streltsov S, McEwen K.A, Sakai H, Yoshimura K, Anisimov V.I, Mori D, Kanno R, Ibberson R. Spin gap in $Tl_2Ru_2O_7$ and the possible formation of Haldane chains in three-dimensional crystals. Nature Materials. 2006; 5:471

[13] Lee K-S, Seo D-K., Whangbo M-H. Structural and Electronic Factors Governing the Metallic and Nonmetallic Properties of the Pyrochlores $A_2Ru_2O_{7-y}$. Journal of Solid State Chemistry. 1997; 131:405-408

[14] Hsu W.Y, Kasowski R.V, Miller T, Chiang T-C. Band structure of metallic pyrochlore ruthenate $Bi_2Ru_2O_7$ and $Pb_2Ru_2O_{6.5}$. Applied Physics Letter. 1988; 52:792

[15] Li L, Kennedy B.J. Structural and Electronic Properties of the Ru Pyrochlores $Bi_{2-y}Yb_yRu_2O_{7-\delta}$. Chemistry of Materials. 2003; 15:4060–4067

[16] Kennedy BJ, Vogt T. Structure and bonding trends in ruthenium pyrochlore. Journal of Solid State Chemistry. 1996; 126:261–270

[17] Takeda T, Kanno R, Kawamoto Y, Takeda Y, Yamamoto O. New Cathode Materials for Solid Oxide Fuel Cells Ruthenium Pyrochlores and Perovskites. Journal of the

Electrochemical Society 2000; 147: 1730-1733

[18] Beyerlein R.A, Horowitz H.S, Longo J.M, Leonowicz M.E, Jorgensen J.D, Rotella F.J. Neutron diffraction investigation of ordered oxygen vacancies in the defect pyrochlores, $Pb_2Ru_2O_{6.5}$ and $PbT_1Nb_2O_{6.5}$. Journal of Solid State Chemistry. 1984; 51:253-265

[19] Ishii F, Oguchi T. Electronic Band Structure of the Pyrochlore Ruthenium Oxides $A_2Ru_2O_7$ (A= Bi, Tl and Y). Journal of the Physical Society of Japan 2000; 69:526-531

[20] Cutler M, Leavy J.F, Fitzpatrick R.L. Electronic transport in semimetallic cerium sulfide. Phys. Rev. 1964; 133: A1143–A1152

[21] Grundmann M. The Physics of Semiconductors; An introduction including Devices and Nanophysics. Heidelberg: Springer, 2006

[22] Bhandari CM, Rowe DM. CRC Handbook of Thermoelectrics (ed. Rowe, D. M.) Ch. 5, 43–53 (CRC, Boca Raton, 1995)

[23] Neophytou N. Theory and simulation methods for electronic and phononic transport in thermoelectric materials, Springer, 2020

[24] Lukas K.C, Liu W.S, Joshi G, Zebarjadi M, Dressehaus M.S, Ren Z.F, Chen G, Opeil C.P. Experimental Determination of the Lorenz Number in $Cu_{0.01}Bi_2Te_{2.7}Se_{0.3}$ and $Bi_{0.88}Sb_{0.12}$. Physical Review B: Condensed Matter Materials Physics 2012; 85:205410

[25] Snyder G.J, Toberer E.S. Complex thermoelectric materials. Nature Materials. 2008; 7:105–114

[26] Thesberg M, Kosina H, Neophytou N. On the Lorenz number of multiband materials. Physical Review B. 2017; 95:125206

[27] Zhao L.D, Lo S.H, Zhang Y, Sun H, Tan G, Uher C, Wolverton C, Dravid V.P, Kanatzidis M.G. Ultralow thermal conductivity and high thermoelectric figure of merit in SnSe crystals. Nature. 2014; 508:373

[28] Völklein F, Reith H, Cornelius T.W, Rauber M, Neumann R. The experimental investigation of thermal conductivity and the Wiedemann-Franz law for single metallic nanowires. Nanotechnology. 2009; 20:325706

[29] Graf M.J, Yip S.K, Sauls J.A, Rainer D. Electronic thermal conductivity and the Wiedemann-Franz law for unconventional superconductors. Physical Review B. 1996; 53:15147

[30] Sun X.F, Lin B, Zhao X, Li L, Komiya S, Tsukada I, Ando Y. Deviation from the Wiedemann-Franz law induced by nonmagnetic impurities in over doped $La_{2-x}Sr_xCuO_4$. Physical Review B. 2009; 80:104510

[31] Thonhauser T, Scheidemantel T.J, Sofo J.O, Badding J.V, Mahan G.D. Thermoelectric properties of Sb_2Te_3 under pressure and uniaxial stress. Physical Review B. 2003; 68:085201

[32] Madsen G.K.H, Schwarz K, Blaha P, Singh D.J. Electronic structure and transport in type-I and type-VIII clathrates containing strontium, barium, and europium. Physical Review B. 2003; 68:125212

[33] Chaput L, Hug G, Pecheur P, Scherrer H. Anisotropy and thermopower in Ti_3SiC_2. Physical Review B. 2005; 71:121104(R)

[34] Lavasani A, Bulmash D, DasSarma S. Wiedemann-Franz law and Fermi liquids. Physical Review B. 2019; 99:085104

[35] Beekman M, Cahill D.G. Inorganic Crystals with Glass-Like and Ultralow Thermal Conductivities. Crystal

Research and Technology. 2017; 52: 1700114

[36] Sathish S, Awasthi O.N. Electron-Electron scattering and low-temperature electrical resistivity in copper and silver. Physics Letter A. 1984; 100:215-217

[37] Yildiz A, Serin N, Serin T, Kasap M. Crossover from Nearest-Neighbor Hopping Conduction to Efros–Shklovskii Variable-Range Hopping Conduction in Hydrogenated Amorphous Silicon Films. Japanese Journal of Applied Physics. 2009; 48:111203

[38] Ashcroft N.W, Mermin N.D. Solid State Physics. Saunders College Publishing, Fort Worth. 1976. p. 657

[39] Sharma S.K, Sagar P, Gupta H, Kumar R, Mehra R.M. Meyer-Neldel rule in Se and S-doped hydrogenated amorphous silicon. Solid State Electronics. 2007; 51:1124-1128

[40] Zvyagin I.P, Kurova I.A, Ormont N. N. Variable range hopping in hydrogenated amorphous silicon. Physica Status Solidi C. 2004; 1:101

[41] Mott N.F, Davis E.A. Electronic Properties in Non-Crystalline Materials (Clarendon Press, Oxford, U.K., 1971)

[42] Efros A.L, Shklovskii B.I. Electronic Properties of Doped Semiconductors (Springer, Berlin, 1984)

[43] Zabrodskii A.G, Zinoveva K.N. Low-temperature conductivity and metal-insulator transition in compensate n-Ge. Journal of Experimental and Theoretical Physics. 1984; 59:425

[44] Liu H, Choe H.S, Chen Y, Suh J, Ko C.h, Tongay S, Wu J. Variable range hopping electric and thermoelectric transport in anisotropic black phosphorus. Applied Physics Letter. 2017; 111:102101

[45] Akhbarifar S, Lutze W, Mecholsky N.A, Pegg I.L. Metal-insulator transition in lead yttrium ruthenate. Materials Chemistry and Physics. 2021; 260:124172

[46] Parrondo J, George M, Capuano Ch, Ayers K.E, Ramani V. Pyrochlore electrocatalysts for efficient alkaline water electrolysis. Journal of Materials Chemistry A. 2015; 3:10819-10828

[47] Song K-W., Lee K-T. Characterization of $Pb_2Ru_{2-x}Bi_xO_7$ (x= 0, 0.2, and 0.4) Pyrochlore Oxide Cathode Materials for Intermediate Temperature Solid Oxide Fuel Cells. Journal of Ceramic Processing Research. 2011; 12:30-33

[48] Akhbarifar S, Lutze W, Mecholsky N.A, Pegg I.L. Glass-like thermal conductivity and other thermoelectric properties of lead ruthenate pyrochlore. Materials Letters. 2020; 272:128153

[49] Sleight A.W. High pressure synthesis of platinum metal pyrochlores of the type $Pb_2M_2O_{6-y}$. Materials Research Bulletin 1971; 6:775-780

[50] Kobayashi H, Kanno R, Kawamoto Y, Kamiyama T, Izumi F, Sleight A.W. Synthesis, Crystal Structure, and Electrical Properties of the Pyrochlores $Pb_{2-x}Ln_xRu_2O_{7-y}$ (Ln= Nd, Gd). Journal of Solid State Chemistry. 1995; 114:15-23

[51] Paschen S, Chapter 15 (Thermoelectric Aspects of Strongly Correlated Electron Systems), in Thermoelectrics Handbook (Editor: Rowe D.M.). 2006

[52] Horowitz H.S, Longo J.M, Lewandowski J.T. New oxide pyrochlores: $A_2[B_{2-x}A_x]O_{7-y}$ (A = Pb, Bi; B = Ru, Ir). Materials Research Bulletins. 1981; 16:489–496

[53] Hwang H.Y, Cheong S-W. Low-field magnetoresistance in the pyrochlore $Tl_2Mn_2O_7$. Nature. 1997; 389:942-944

[54] Bramwell S.T, Gingras M.J.P. Spin ice state in frustrated magnetic pyrochlore. Science. 2001; 294:1495-1501

[55] Sidharth D, Alagar Nedunchezhian A., Rajkumar R, Yalini Devi N, Rajasekaran P, Arivanandhan M, Fujiwara K, Anbalaganb G, Jayavel R. Enhancing effects of Te substitution on the thermoelectric power factor of nanostructured $SnSe_{1-x}Te_x$. Physical Chemistry Chemical Physics. 2019; 21: 15725-15733

[56] Tse J.S, Uehara K, Rousseau R, Ker A, Ratcliffe CI, White MA, MacKay G. Structural Principles and Amorphous like Thermal Conductivity of Na-Doped Si Clathrates. Physical Review Letter. 2000; 85:114-117

[57] Damodara Das V, Soundararajan N. Size and temperature effects on the Seebeck coefficient of thin bismuth films. Physical Review B. 1987; 35: 5990-5996

[58] Goldsmid H.J, Sharp J.W. Estimation of the thermal band gap of a semiconductor from Seebeck measurements. Journal of Electron Materials 1999; 28:869-872

[59] Beekman M, Cahill D.G. Inorganic Crystals with Glass-Like and Ultralow Thermal Conductivities. Crystal Research and Technology. 2017; 52: 1700114

[60] Skoug E.J, Morelli D.T. Role of Lone-Pair Electrons in Producing Minimum Thermal Conductivity in Nitrogen-Group Chalcogenide Compounds. Physical Review Letter. 2011; 107:235901

[61] Zhang Y, Skoug E, Cain J, Ozoliņš V, Morelli D, Wolverton C. First-principles description of anomalously low lattice thermal conductivity in thermoelectric Cu-Sb-Se ternary semiconductors. Physical Review B. 2012; 85:054306

[62] Nielsen M.D, Ozolins V, Heremans J.P. Lone-pair electrons minimize lattice thermal conductivity, Energy Environ. Science. 2013; 6: 570-578

[63] Dong Y, Khabibullin A.R, Wei K, Salvador J.R, Nolas G.S, Woods L.M. Bournonite $PbCuSbS_3$: stereochemically active lone-pair electrons that induce low thermal conductivity. ChemPhysChem. 2015; 16:3264 -70

[64] Schelling P.K, Phillpot S.R. Mechanism of Thermal Transport in Zirconia and Yttria-Stabilized Zirconia by Molecular-Dynamics Simulation. Journal of American Ceramic Society. 2001; 84:2997

[65] Shklovskii B.I, Efros A.L. Electronic Properties of Doped Semiconductors. Springer, London. 1984

[66] Park T.E, Suh J, Seo D, Park J, Lin D. Y, Huang Y.S, Choi H.J, Wu J, Jang C, Chang J. Hopping conduction in p-type MoS_2 near the critical regime of the metal-insulator transition. Applied Physics Letter. 2015; 107:223107

[67] Mott N.F. The metallic and Nonmetallic States of Matter. (P. P. Edwards and C. N. R. Rao, Eds.), p. 1, Taylor and Francis, London/ Philadelphia. 1985